Synthetic Inertial Control of Wind Farm with BESS Based on Model Predictive Control

Bao, Weiyu; Wu, Qiuwei; Ding, Lei; Huang, Sheng; Teng, Fei; Terzija, Vladimir

Published in:
I E T Renewable Power Generation

Link to article, DOI:
10.1049/iet-rpg.2019.0885

Publication date:
2020

Document Version
Peer reviewed version

IET Research Journals

Research Article

IET Journals
The Institution of Engineering and Technology

Synthetic Inertial Control of Wind Farm with BESS Based on Model Predictive Control

ISSN 1751-8644
doi: 0000000000
www.ietdl.org

Weiyu Bao[1], *Qiuwei Wu*[2*], *Lei Ding*[1], *Sheng Huang*[2], *Fei Teng*[3], *Vladimir Terzija*[4]

[1] *Key Laboratory of Power System Intelligent Dispatch and Control of Ministry of Education, School of Electrical Engineering, Shandong University, Ji'nan 250061, People's Republic of China*
[2] *Department of Electrical Engineering, Technical University of Denmark, Copenhagen, Denmark*
[3] *Department of Electrical and Electronic Engineering, Imperial College London, London, U.K.*
[4] *School of Electrical and Electronic Engineering, The University of Manchester, Manchester M13 9PL, U.K.*
** E-mail: qw@elektro.dtu.dk*

Abstract: Wind farms (WFs) can provide controlled inertia through synthetic inertial control (SIC) to support system frequency recovery after disturbances. This paper proposes a model predictive control (MPC) based SIC for a WF consisting of wind turbines (WTs) and a battery storage energy system (BESS). In the proposed MPC-SIC, the active power output of the WTs and BESS during the SIC are optimally coordinated in order to avoid over-deceleration of the WTs' rotor, and minimize the loss of extracted wind energy during the SIC and degradation cost of the BESS. The IEEE 39 bus system with a WF consisting of 100 WTs and a BESS is used to validate the performance of the proposed MPC-SIC. Case studies show that, compared with the conventional SIC, the minimum rotor speed among all WTs with MPC-SIC can be improved by 0.08-0.11 p.u., the loss of captured wind energy of WF with MPC-SIC can be reduced by 12%-64% and the degradation cost of the BESS with MPC-SIC can be reduced by 72%-83%. The results proves that with the proposed MPC-SIC, the wind farm can avoid the over-deceleration of the WTs' rotor and reduce the operation cost of the WF by improving the efficiency of wind energy usage and lifetime of the BESS.

List of Abbreviations

BESS	battery energy storage system
DFIG	doubly-fed induction generator
MPC	Model predictive control
MPC-SIC	MPC based synthetic inertial control
MPPT	maximum power point tracking
PCC	point of common coupling
QP	quadratic-programming
RES	renewable energy source
RoCoF	rate of change of frequency
SIC	synthetic inertial control
SOC	state-of-charge
SOE	index of state of energy
TSO	transmission system operator
WF	wind farm
WT	wind turbine

Nomenclature

β	pitch angle of the WT
$\Delta\omega_{\mathrm{r,ave}}$	average rotor speed of all WTs in the WF
$\Delta\omega_{\mathrm{r}}$	change of the rotor speed of the WT during one control period
Δf	frequency deviation at the PCC of the WF
ΔP_{ref}	total incremental power of the WF during inertial control process
$\Delta P_{\mathrm{ref}}^{\mathrm{ESS}}$	incremental power of the BESS
$\Delta P_{\mathrm{ref},i}$	incremental power of the ith WT
ΔT_{P}	prediction horizon of MPC-SIC
γ_{ESS}	rated cycle life of ESS
λ	tip speed ratio of the WT
λ_{ω}	weighting coefficient for the objective of improving the minimum rotor speed of all WTs
λ_B	weighting coefficient for the objective of minimizing the degradation of the BESS
λ_E	weighting coefficient for the objective of minimizing the loss of captured wind energy
μ_{ESS}	capital cost of ESS
ω_{r0}	initial rotor speed of the WT during one control period
$\omega_{\mathrm{r},i}$	rotor speed of the ith WT
ρ	air density
a_{1-4}	coefficients of the ESS life cycle
C_{p}	power coefficient of the WT
E_R	capacity of ESS
$E_{\mathrm{loss},i}$	loss of captured wind energy of the ith WT during inertial control process
f_{mea}	frequency measured from the PCC of the WF
f_{ref}	nominal system frequency
H_{t}	inertia constant of the WT
i_{D}	DC-current of the BESS
k_{pd}, k_{id}	proportional and integral gains of the PI controller of the DC-current control loop of BESS
$K_{\mathrm{p}}, K_{\mathrm{d}}$	control parameters of the synthetic inertial controller
$P_{\mathrm{charge,max}}^{\mathrm{ESS}}$	charge power limit of the BESS
$P_{\mathrm{discharge,max}}^{\mathrm{ESS}}$	discharge power limit of the BESS
$P_{\mathrm{max},i}$	capacity of the ith WT generator
$P_{\mathrm{e}}^{\mathrm{ESS}}$	active power output of the BESS
P_{int}	integral of the error between $P_{\mathrm{ref}}^{\mathrm{ESS}}$ and $P_{\mathrm{e}}^{\mathrm{ESS}}$
P_{m}	mechanical power of the WT
P_{ref}	active power output of the WT calculated by the MPPT function
$P_{\mathrm{e},i}$	active power output of the ith WT
Q_{c}	capacity of BESS
R	rotor blade radius of the WT

SOC^0	initial SOC level of ESS
SOC^{ref}	SOC reference of ESS
T_{c}	control period of MPC-SIC
T_{ESS}	temperature of the BESS
$T_{\mathrm{id}}, T_{\mathrm{fd}}$	time constants of the active power control loop and DC-current control loop of BESS
U_{D}	DC-voltage of BESS
$v_{\mathrm{w},i}$	wind speed of the ith WT
Z_{i}	internal resistance of BESS
$N\mathrm{c}$	number of the WT clusters in the WF
$N\mathrm{w}$	number of the WTs in the WF

1 Introduction

With the rapid development of renewable energy sources (RESs), an increasing number of conventional power plants in the power system are replaced by wind farms (WFs). Since the rotor speed of the inverter-based wind turbines (WTs) is decoupled from the system frequency, WTs do not inherently contribute to system inertia. Consequently, with high penetration of wind power generation, the inertia of the power system is decreasing. This threatens system frequency stability and leads to a higher risk of under-frequency load shedding and possibly even cascading outages. In recent years, the problem of reduced system inertia caused by high penetration of wind power has drawn considerable attention [1].

To address the problem of decreasing inertia, synthetic inertial control (SIC) of WTs was proposed [2]. The concept is to increase the power output by releasing the kinetic energy stored in the rotating mass of the WT temporarily after disturbances in order to contribute to system frequency recovery. Over the past years, the effect of SIC on the power system has been widely investigated [3]-[5]. Furthermore, SIC has been designed and implemented by WT manufacturers in their new products [6],[7].

SIC can significantly improve the system frequency response after disturbances mainly for two reasons: 1) The kinetic energy stored in the rotating mass of WTs is higher than that in conventional synchronous generators [8]. 2) Since the rotor speed of WTs is decoupled from the system frequency, it can operate in a wider range. Take the doubly-fed induction generator (DFIG) based WT for example, its rotor speed can vary in the range of 0.7 p.u. to 1.2 p.u. If the rotor speed drops from 1.0 p.u. to 0.7 p.u., more than half of the kinetic energy can be released to the power system and contribute to system frequency recovery after disturbances.

However, the SIC also has some shortcomings. Firstly, during SIC, the rotor speed of the WT may decelerate to the minimum threshold. Then, the WT has to terminate the SIC and switch back to the normal operating mode to recover the rotor speed, leading to decreased power output. This termination can cause a severe system frequency drop which is called “secondary frequency drop" [9]. Therefore, to mitigate the secondary frequency drop, it is necessary to avoid the over-deceleration of the rotor speed of the WT. Secondly, in normal operating conditions, the WT operates in maximum power point tracking (MPPT) mode, which means that the wind power captured by the WT is the highest at the MPPT point. During SIC, due to the deceleration of the rotor speed, the operating point of the WTs will deviate from the MPPT point, which causes loss of the wind energy captured by the WT [9]. The wind energy loss results in a considerable reduction of the annual profit of the WF. Therefore, it should be minimized during the SIC.

In recent years, a considerable number of studies have been done to address the aforementioned shortcomings of the SIC of WTs. The over-deceleration of the WT's rotor speed can be avoided by adopting variable control parameters of the SIC [10]-[15]. In [10], the parameters of the SIC were tuned based on the WT's operating point to ensure the stable operation of the WT. In [11], a variable SIC controller based on the rate of change of frequency (RoCoF) of the system was proposed. When the RoCoF is too severe, the WT reduces its power output by changing the coefficient of emulated inertia in order to keep the WT's rotor speed in a safe range. In [12], the concept of “stability boundary" of the WT was proposed. The droop coefficient of the SIC controller was tuned to ensure that the WT can be kept within the stable region where the rotor speed is in its allowed range during the SIC. In [13]-[15], an adaptive gain was applied to the SIC controller based on both the RoCoF of the system and the rotor speed of the WT to ensure the stable operation of the WT under various wind and disturbance conditions. Moreover, various approaches have been proposed to reduce the loss of captured wind energy during the SIC. In [16], a linear-quadratic regulator based adaptive inertial control scheme was proposed with the objective of guaranteeing an optimal balance between the inertial response provision and the required energy use. Accordingly, the loss of captured wind energy can be reduced. In [17], the captured wind power during the SIC was accurately estimated based on an extended state observer. Then a novel rotor speed recovery strategy was proposed to restore the rotor speed quickly after the SIC and reduce the loss of captured wind power. In [18], the impact of the SIC on harvested wind energy was minimized by firstly extracting DC-link capacitor energy and subsequently rotor kinetic energy during the SIC. In [19], the droop gain of the SIC was adaptively adjusted according to WTs' rotor speed to harvest as much wind energy as possible during over-frequency disturbances. An index of state of energy (SOE) was defined in [20], which can adequately exploit the kinetic energy of WTs and reduce the loss of captured wind energy during the SIC. In [21], the loss of captured wind energy was minimized by formulating the SIC as an optimal control problem.

Due to the flexible charging and discharging characteristics of battery energy storage systems (BESSs), the combined operation of WTs and a BESS in a WF has been recognized as a feasible and effective way to suppress the wind power fluctuations [22],[23] and also help WTs improve the performance of the SIC [24]-[28]. As mentioned in [23], compared with the conventional WF without BESSs, the WF equipped with a BESS can have a better performance of power reference tracking from power system operators, and the mechanical load of WTs can also be alleviated. In [24], a RoCoF-based inertia emulation control for BESSs was proposed to enhance the inertia of the power system and its effectiveness was validated on an experimental test-bed. In [25], a coordination control scheme between the BESS and the WT was proposed to expedite the WT's rotor speed recovery after the SIC by fully taking advantage of the BESS's fast and accurate active power control ability. In [26], a control strategy for a WT equipped with a BESS during inertial response provision was proposed in order to support the power system in maintaining the frequency within the normal operating range. In [27], a fuzzy-logic based coordinated SIC strategy for a WT-BESS system was designed so that its capability of inertial response is adaptive for various wind speed conditions. In [28], an control strategy was proposed to optimally coordinate the BESSs, WTs, and photovoltaic systems during frequency regulation of a power system with high penetration of RESs.

For the SIC of WTs, although different approaches have been proposed to address the shortcomings of the SIC, most of the research focuses on a single WT to provide an inertial response, while the coordination among WTs in a WF has not been fully studied. Furthermore, the model of the WT equipped with the SIC is a highly nonlinear model. When the WT experiences large deviations from its normal operating point during the SIC, the proposed approaches in the existing studies designed with a linearized model of the WT may not achieve a good performance since the dynamic change of the WF cannot be precisely predicted. For the combined operation of WTs and a BESS in a WF during SIC, the existing studies focus on the improvement of the control performance of the SIC without considering the impact on the lifetime of the BESS. As mentioned in [29], different control strategies have a significant influence on the lifetime of the BESS. Therefore, considering the high cost of the BESS, it is necessary to balance the degradation of the BESS and the control performance of the SIC of the WF. To fill the research gap, it is necessary to develop a new inertial control scheme that can be applied at the WF level to achieve coordination of the WTs/BESS and can precisely predict the dynamic change of the WF to achieve good control performance. The control scheme should also overcome the

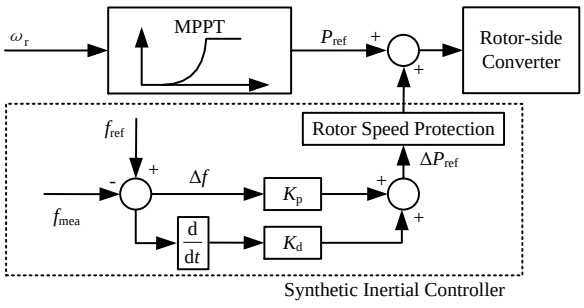

Fig. 1: Structure of conventional SIC of WTs.

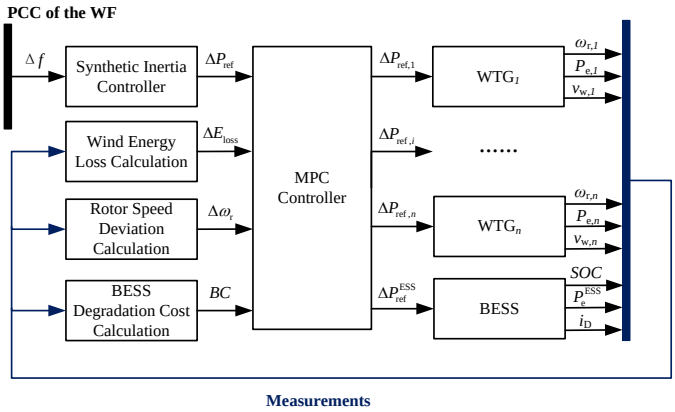

Fig. 2: Structure of MPC-SIC.

aforementioned shortcomings of the SIC of the WT and reduce the degradation cost of the BESS.

Model predictive control (MPC) is an advanced control method that can be used to control a process while satisfying a set of control constraints. In recent years, MPC has been extensively applied in WFs for active and reactive power control [30]-[32]. The advantage of MPC is that it is applicable at the WF level. Therefore, coordination of the WTs and BESS with different operating conditions can be achieved. Furthermore, although the WF model is a nonlinear model, it can be considered to be a linearized model over the prediction horizon of the MPC. Using the linearized predictive model and the latest measurements of the state variables, the dynamic change of the control process can be precisely predicted and updated. Therefore, the control performance can be improved with MPC compared with traditional control methods.

The main objective of this paper is to propose a novel MPC based SIC strategy (MPC-SIC) for a WF with a BESS in order to avoid over-deceleration of the WTs' rotor speed, minimize the loss of extracted wind energy and reduce degradation cost of the BESS during the SIC. During the control process, the MPC controller collects the measurements from individual WTs and BESS, predicts their dynamic changes, and regulates their active power outputs in order to achieve the control objectives. Main contributions of this paper can be summarized as follows:

1. A predictive model of the WF consisting of WTs and a BESS is developed. The predictive model can precisely predict the dynamic change of the WTs and BESS over the predictive horizon of the MPC-SIC.
2. The MPC-SIC is designed for the WF. Compared with conventional approaches, the MPC-SIC is implemented at the WF level. Thus, the active power outputs of the WTs and the BESS can be coordinated. The differences and variations of the operating conditions of the WTs and the BESS are also taken into account to improve the control performance.
3. The optimization problem for the MPC-SIC is formulated. Compared with conventional SIC, the MPC-SIC mitigates the secondary frequency drop and the operation cost of the WF by solving the formulated optimization problem in each control period.

The rest of this paper is organized as follows: In Section 2, the structure of the MPC-SIC is presented. In Section 3, the predictive models of the WT, BESS and WF are developed. In Section 4, the mathematical formulation of the MPC-SIC is derived. Section 5 presents the simulation results and followed by the conclusions.

2 Control Structure of MPC-SIC

2.1 Control Structure of SIC for WT

The structure of the conventional SIC of WTs is illustrated in Fig. 1 [2]. During normal operation, the WT operates in the MPPT mode and its active power reference $P_{\rm ref}$ is calculated by the MPPT function based on its rotor speed $\omega_{\rm r}$ and sent to the rotor-side converter. $f_{\rm ref}$ is the nominal system frequency, and $f_{\rm mea}$ is the measured system frequency. After the disturbance, the power system experiences a frequency excursion, causing a frequency deviation $\Delta f = f_{\rm ref} - f_{\rm mea}$. The synthetic inertial controller of the WT then calculates an incremental active power reference $\Delta P_{\rm ref}$ which is in proportion to Δf and RoCoF $\mathrm{d}f/\mathrm{d}t$, and add it to $P_{\rm ref}$. When the rotor speed of the WT decreases to the threshold, the rotor speed protection will be activated, terminating the SIC by setting $\Delta P_{\rm ref}$ as 0, and then the rotor speed will recover to the normal operating speed.

2.2 Control Structure of SIC for BESS

The conventional SIC of the WT can also be applied to the BESS. However, two main differences need to be considered: Firstly, during normal operation, the active power reference for the BESS is calculated by the WF to compensate the power mismatch between the actual output of the WF and the set-point from the transmission system operator (TSO). Secondly, the termination of the SIC happens when the state-of-charge (SOC) of the BESS exceeds the feasible range.

2.3 Control Structure of MPC-SIC

Instead of calculating $\Delta P_{\rm ref}$ locally at the WT/BESS level, this paper proposes an MPC-SIC which calculates $\Delta P_{\rm ref}$ of the WTs and the BESS at the WF level.

The structure of the MPC-SIC is illustrated in Fig. 2. The frequency deviation Δf is measured from the point of common coupling (PCC) of the WF, and the total incremental power of the WF $\Delta P_{\rm ref}$ is then calculated by the synthetic inertial controller which is the same as the local controller in Fig. 1. The loss of captured wind energy of the whole WF and the rotor speed deviation of the WTs during the next prediction horizon will then be predicted based on the operating condition (including rotor speed $\omega_{{\rm r},i}$, active power $P_{{\rm e},i}$, and wind speed $v_{{\rm w},i}$ measured at each WT) of the WTs. Meanwhile, the degradation cost of the BESS during next prediction horizon will be predicted based on the operating condition (including SOC, active power $P_{\rm e}^{\rm ESS}$ and the DC-current $i_{\rm D}$ measured at the BESS) of the BESS. Afterwards, the incremental power of the WTs $\Delta P_{{\rm ref},i}$ and BESS $\Delta P_{\rm ref}^{\rm ESS}$ will be calculated by the MPC controller and be sent to the WTs and BESS. The control objectives of the MPC-SIC are to improve the minimum rotor speed of all WTs, minimize the loss of captured wind energy, and minimize the degradation cost of the BESS. The cost functions with regards to the objectives are presented in 4.2. To achieve the control objectives, $\Delta P_{{\rm ref},i}$ of the WTs and $\Delta P_{\rm ref}^{\rm ESS}$ of the BESS must be coordinated and adjusted according to the different operating conditions. $\Delta P_{\rm ref}$ calculated by the synthetic inertial controller at the WF level need to be satisfied as an equality constraint during the control process.

3 Predictive Modelling

In this section, the predictive models of the WT, BESS and WF are derived in detail. To realize the control objectives presented in 4.2, the state variables of the WT's model are the rotor speed and the active power output of the WT, and the state variables of the BESS's model are SOC, active power output, integral of the error between active power output and reference power, and DC side current of the BESS.

3.1 Modelling of WT

The captured mechanical power by the WT can be expressed by,

$$P_{\mathrm{m}} = \frac{1}{2}\rho\pi R^2 C_{\mathrm{p}}(\lambda,\beta)v_{\mathrm{w}}^3 \tag{1}$$

$$\begin{aligned} C_p(\lambda,\beta) &= 0.22(\frac{116}{\lambda_{\mathrm{i}}} - 0.4\beta - 5)e^{\frac{-12.5}{\lambda_{\mathrm{i}}}} \\ \frac{1}{\lambda_{\mathrm{i}}} &= \frac{1}{\lambda + 0.08\beta} - \frac{0.035}{\beta^3 + 1} \end{aligned} \tag{2}$$

Normally, β is set as zero when the active power of the WT is below the rated power. Thus C_{p} is a function of λ only and it can be fitted as a 3-order polynomial function,

$$C_{\mathrm{p}} = m_1\lambda^3 + m_2\lambda^2 + m_3\lambda + m_4 \tag{3}$$

Since λ is a function of rotor speed ω_{r},

$$\lambda = \frac{\omega_{\mathrm{r}} R}{v_{\mathrm{w}}} \tag{4}$$

the mechanical power of the WT can be expressed as,

$$P_{\mathrm{m}} = n_1\omega_{\mathrm{r}}^3 + n_2\omega_{\mathrm{r}}^2 v_{\mathrm{w}} + n_3\omega_{\mathrm{r}}v_{\mathrm{w}}^2 + n_4 v_{\mathrm{w}}^3 \tag{5}$$

where,

$$\begin{aligned} n_1 &= \frac{1}{2}\pi R^5 m_1,\ n_2 = \frac{1}{2}\pi R^4 m_2 \\ n_3 &= \frac{1}{2}\pi R^3 m_3,\ n_4 = \frac{1}{2}\pi R^2 m_4 \end{aligned} \tag{6}$$

Equation (5) is used to calculate the initial mechanical power P_{m0}. The swing equation of the WT generator is,

$$\frac{\mathrm{d}\omega_{\mathrm{r}}}{\mathrm{d}t} = \frac{P_{\mathrm{m}} - P_{\mathrm{e}}}{2H_{\mathrm{t}}\omega_{\mathrm{r}}} \tag{7}$$

During one control period,

$$\omega_{\mathrm{r}} = \omega_{\mathrm{r0}} + \Delta\omega_{\mathrm{r}} \tag{8}$$

Thus (7) can be written as,

$$\frac{\mathrm{d}(\omega_{\mathrm{r0}} + \Delta\omega_{\mathrm{r}})}{\mathrm{d}t} = \frac{\mathrm{d}\Delta\omega_{\mathrm{r}}}{\mathrm{d}t} = \frac{P_{\mathrm{m}} - P_{\mathrm{e}}}{2H_{\mathrm{t}}(\omega_{\mathrm{r0}} + \Delta\omega_{\mathrm{r}})} \tag{9}$$

Using the Taylor expansion of (9), the rate of change of the rotor speed can be approximated as,

$$\begin{aligned} \frac{\mathrm{d}\Delta\omega_{\mathrm{r}}}{\mathrm{d}t} =& \left(\frac{P_{\mathrm{m}}}{2H_{\mathrm{t}}\omega_{\mathrm{r0}}} - \frac{P_{\mathrm{m}}}{2H_{\mathrm{t}}\omega_{\mathrm{r0}}^2}\Delta\omega_{\mathrm{r}}\right) \\ &- \left(\frac{P_{\mathrm{e0}} + \Delta P_{\mathrm{e}}}{2H_{\mathrm{t}}\omega_{\mathrm{r0}}} - \frac{P_{\mathrm{e0}}}{2H_{\mathrm{t}}\omega_{\mathrm{r0}}^2}\Delta\omega_{\mathrm{r}}\right) \\ =& \frac{P_{\mathrm{e0}} - P_{\mathrm{m}}}{2H_{\mathrm{t}}\omega_{\mathrm{r0}}^2}\Delta\omega_{\mathrm{r}} + \frac{P_{\mathrm{m}} - (P_{\mathrm{e0}} + \Delta P_{\mathrm{e}})}{2H_{\mathrm{t}}\omega_{\mathrm{r0}}} \end{aligned} \tag{10}$$

During the SIC, due to the fast tracking capability of the active power control system of the WT, the change of the WT's active power can quickly track the reference ΔP_{ref}, and during one control period T_{c}, the rate of change of active power can be assumed to be constant, i.e.,

$$\frac{\mathrm{d}P_{\mathrm{e}}}{\mathrm{d}t} = -\frac{\Delta P_{\mathrm{ref}}}{T_{\mathrm{c}}} \tag{11}$$

For each cluster, its predictive model can be formulated as,

$$\begin{aligned} \Delta\dot{x}_i &= \boldsymbol{A_i}\Delta x_i + \boldsymbol{B_i}\Delta u_i + \boldsymbol{E_i} \\ \Delta y_i &= \boldsymbol{C_i}\Delta x_i \end{aligned} \tag{12}$$

where,

$$\begin{aligned} \Delta x_i &= [\Delta\omega_{\mathrm{r},i} \quad \Delta P_{\mathrm{e},i}]^{\mathrm{T}} \\ \Delta u_i &= [\Delta P_{\mathrm{ref},i}], \quad \Delta y_i = [\Delta\omega_{\mathrm{r},i} \quad \Delta P_{rme,i}]^{\mathrm{T}} \\ \boldsymbol{A_i} &= \begin{bmatrix} \frac{P_{\mathrm{e0},i} - P_{\mathrm{m0},i}}{2H_{\mathrm{t}}\omega_{\mathrm{r0},i}^2} & \frac{1}{2H_{\mathrm{t}}\omega_{\mathrm{r0},i}} \\ 0 & \frac{-1}{T_{\mathrm{c}}} \end{bmatrix} \\ \boldsymbol{B_i} &= \begin{bmatrix} 0 \\ \frac{-1}{T_{\mathrm{c}}} \end{bmatrix}, \quad \boldsymbol{E_i} = \begin{bmatrix} \frac{P_{\mathrm{m0},i} - P_{\mathrm{e0},i}}{2H_{\mathrm{t}}\omega_{\mathrm{r0},i}} \\ 0 \end{bmatrix} \\ \boldsymbol{C_i} &= [1 \quad 1] \end{aligned} \tag{13}$$

3.2 Modeling of BESS

The BESS model used in this paper is from [33]. The SOC of the battery is described as the integral of DC-current.

$$SOC = SOC^0 - \frac{1}{Q_{\mathrm{c}}}\int i_{\mathrm{D}}\mathrm{d}t \tag{14}$$

The dynamic behaviour of the control loops for active power and DC-current is described by first-order lag functions.

$$\begin{aligned} \Delta i_{\mathrm{D}} &= \frac{1}{1 + sT_{\mathrm{id}}}\left(k_{\mathrm{pd}} + \frac{k_{\mathrm{id}}}{s}\right)\left(\Delta P_{\mathrm{ref}}^{\mathrm{ESS}} - \Delta P_{\mathrm{e}}^{\mathrm{ESS}}\right) \\ \Delta P_{\mathrm{e}}^{\mathrm{ESS}} &= \frac{1}{1 + sT_{\mathrm{fd}}}U_D\Delta i_{\mathrm{D}} \end{aligned} \tag{15}$$

For the convenience of building the state space model for the BESS, a state variable P_{int} is introduced as the integral of the error between $P_{\mathrm{ref}}^{\mathrm{ESS}}$ and $P_{\mathrm{e}}^{\mathrm{ESS}}$.

$$\Delta P_{\mathrm{int}} = \frac{\Delta P_{\mathrm{ref}}^{\mathrm{ESS}} - \Delta P_{\mathrm{e}}^{\mathrm{ESS}}}{s} \tag{16}$$

The state space model of the BESS in a matrix form can be obtained as,

$$\begin{aligned} \Delta\dot{x}_{\mathrm{E}} &= \boldsymbol{A_{\mathbf{E}}}\Delta x_{\mathrm{E}} + \boldsymbol{B_{\mathbf{E}}}\Delta u_{\mathrm{E}} + \boldsymbol{E_{\mathbf{E}}} \\ \Delta\dot{y}_{\mathrm{E}} &= \boldsymbol{C_{\mathbf{E}}}\Delta x_{\mathrm{E}} \end{aligned} \tag{17}$$

where,

$$\Delta x_{\mathrm{E}} = [\Delta SOC \quad \Delta P_{\mathrm{e}}^{\mathrm{ESS}} \quad \Delta P_{\mathrm{int}} \quad \Delta i_{\mathrm{D}}]^{\mathrm{T}}$$
$$\Delta u_{\mathrm{E}} = \Delta P_{\mathrm{ref}}^{\mathrm{ESS}}, \quad \Delta y_{\mathrm{E}} = [\Delta SOC \quad \Delta P_{\mathrm{e}}^{\mathrm{ESS}}]^{\mathrm{T}}$$
$$\boldsymbol{A_{\mathrm{E}}} = \begin{bmatrix} 0 & 0 & 0 & -\frac{1}{Q_{\mathrm{c}}} \\ 0 & -\frac{1}{T_{\mathrm{fd}}} & 0 & \frac{U_{\mathrm{D}}}{T_{\mathrm{fd}}} \\ 0 & -1 & 0 & 0 \\ 0 & -\frac{k_{\mathrm{pd}}}{T_{\mathrm{id}}} & \frac{k_{\mathrm{id}}}{T_{\mathrm{id}}} & -\frac{1}{T_{\mathrm{id}}} \end{bmatrix} \tag{18}$$
$$\boldsymbol{B_{\mathrm{E}}} = \begin{bmatrix} 0 \\ 0 \\ 1 \\ \frac{k_{\mathrm{pd}}}{T_{\mathrm{id}}} \end{bmatrix}, \quad \boldsymbol{E_{\mathrm{E}}} = \begin{bmatrix} -\Delta i_{\mathrm{D}}^{0} \\ 0 \\ 0 \\ 0 \end{bmatrix}$$
$$\boldsymbol{C_{\mathrm{E}}} = \begin{bmatrix} 1 & 0 & 0 & 0 \\ 0 & 1 & 0 & 0 \end{bmatrix}$$

U_{D} could be assumed as linearly dependent on the SOC.

$$U_{\mathrm{D}} = U_{\max} SOC + U_{\min}(1 - SOC) - i_{\mathrm{D}} Z_{\mathrm{i}} \tag{19}$$

Z_{i} can be assumed as constant since it is very small due to the high current. Therefore, the SOC can be calculated from the measurement of the U_{D},

$$SOC = \frac{U_{\mathrm{D}} + i_{\mathrm{D}} Z_{\mathrm{i}} - U_{\min}}{U_{\max} - U_{\min}} \tag{20}$$

3.3 Modeling of WF

Based on the model of the WT and BESS, the continuous state space model of the WF with N_{c} WT clusters and a BESS can be formulated as,

$$\begin{aligned} \Delta \dot{x} &= \boldsymbol{A}\Delta x + \boldsymbol{B}u + \boldsymbol{E} \\ \Delta y &= \boldsymbol{C}\Delta x \end{aligned} \tag{21}$$

where,

$$\begin{aligned} \Delta x &= \left[\Delta x_1, \Delta x_2, \ldots, \Delta x_{N\mathrm{c}}, \Delta x_E\right]^{\mathrm{T}} \\ \Delta u &= \left[\Delta u_1, \Delta u_2, \ldots, \Delta u_{N\mathrm{c}}, \Delta u_E\right]^{\mathrm{T}} \\ \Delta y &= \left[\Delta y_1, \Delta y_2, \ldots, \Delta y_{N\mathrm{c}}, \Delta y_E\right]^{\mathrm{T}} \\ \boldsymbol{A} &= diag\left[\boldsymbol{A_1}, \boldsymbol{A_2}, \ldots, \boldsymbol{A_{Nc}}, \boldsymbol{A_{\mathrm{E}}}\right] \\ \boldsymbol{B} &= diag\left[\boldsymbol{B_1}, \boldsymbol{B_2}, \ldots, \boldsymbol{B_{Nc}}, \boldsymbol{B_{\mathrm{E}}}\right] \\ \boldsymbol{E} &= diag\left[\boldsymbol{E_1}, \boldsymbol{E_2}, \ldots, \boldsymbol{E_{Nc}}, \boldsymbol{E_{\mathrm{E}}}\right] \\ \boldsymbol{C} &= diag\left[\boldsymbol{C_1}, \boldsymbol{C_2}, \ldots, \boldsymbol{C_{Nc}}, \boldsymbol{C_{\mathrm{E}}}\right] \end{aligned} \tag{22}$$

Based on the continuous model, the discrete-time state space model with sampling time ΔT_{P} can be expressed as,

$$\begin{aligned} \Delta x(k+1) &= \boldsymbol{G}\Delta x(k) + \boldsymbol{H}u(k) + \boldsymbol{E} \\ \Delta y(k+1) &= \boldsymbol{C}\Delta x(k+1) \end{aligned} \tag{23}$$

where,

$$\boldsymbol{G} = e^{\boldsymbol{A}\Delta T_{\mathrm{P}}}, \boldsymbol{H} = \int_0^{\Delta T_{\mathrm{P}}} e^{\boldsymbol{A}\tau}\boldsymbol{B}\mathrm{d}\tau \tag{24}$$

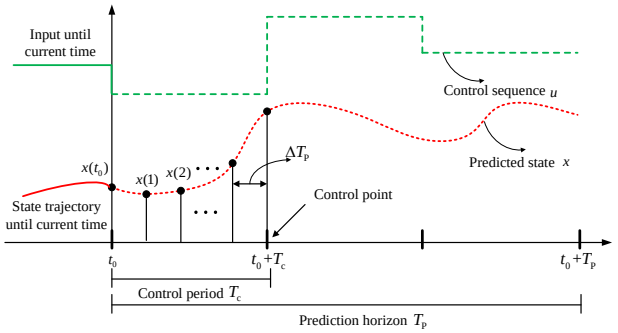

Fig. 3: Principle of MPC.

4 Formulation of MPC-SIC

In this section, the mathematical formulation of the MPC-SIC is presented. The control objectives are to improve the minimum rotor speed of all WTs, minimize the loss of wind energy and minimize the degradation cost caused by charging and discharging of the BESS during the SIC.

4.1 MPC Principle

MPC is a widely used control method. In the MPC, the control input is obtained by solving a discrete-time optimal control problem over a given horizon. An optimal control input sequence is calculated, while only the first control action is applied.

The principle of the MPC is illustrated in Fig. 3. The whole SIC process normally lasts for 10∼20 seconds. To predict the dynamics of the WF during the SIC, T_{c} is smaller than the duration of the SIC process, but larger than the sampling time of the measurements. The suitable prediction horizon is determined by the dynamic performance of the control system. For a prediction horizon, the control actions are only changed at the beginning of the control period and maintained within the control period.

4.2 Cost Function

The cost functions of the MPC-SIC are presented as follows:

Objective 1: The first objective is to improve the minimum rotor speed of all WTs. During normal operation, the WTs operate in the MPPT mode, and their rotor speeds vary with the wind speeds. During the SIC, the WTs increase their active power output by releasing kinetic energy stored in their rotating masses and consequently decrease their rotor speeds due to the mismatch between their mechanical and electrical power. As mentioned before, the minimum rotor speed of the WTs during the SIC represents the risk of abrupt termination of the SIC. For the WTs in low wind speed conditions, they cannot provide much additional active power because their rotor speeds are already very low and the deceleration of their rotors will cause the termination of the SIC. To improve the minimum rotor speed, the difference of the rotor speeds among the WTs is minimized, meaning that all WTs during the SIC converge to the same rotor speed. The cost function of the first objective can be described by,

$$\mathrm{Obj}_1 = \sum_{i=1}^{N_{\mathrm{w}}} \sum_{k=1}^{N_{\mathrm{p}}} \left\| \Delta\omega_{\mathrm{r},i}(k) - \Delta\omega_{\mathrm{r,ave}}(k) \right\|^2 \tag{25}$$

Objective 2: The second objective is to minimize the loss of captured wind energy caused by the deceleration of the WTs' rotors, thus its cost function can be described by,

$$\mathrm{Obj}_2 = \sum_{i=1}^{N_{\mathrm{w}}} \sum_{k=1}^{N_{\mathrm{p}}} E_{\mathrm{loss},i}(k) \tag{26}$$

$E_{\text{loss},i}$ can be approximated as [34],

$$\begin{aligned} E_{\text{loss},i} = &\frac{1}{4}\rho\pi R^2 v_{\text{w},i}^3 \frac{R}{v_{\text{w},i}} \frac{\partial C_{\text{p},i}}{\partial \lambda_i}\bigg|_{t=0} T_{\text{c}}\Delta\omega_{\text{r},i} \\ &+ \frac{1}{12}\rho\pi R^2 v_{\text{w},i}^3 \left(\frac{R}{v_{\text{w},i}}\right)^2 \frac{\partial^2 C_{\text{p},i}}{\partial \lambda_i^2}\bigg|_{t=0} T_{\text{c}}\Delta\omega_{\text{r},i}^2 \end{aligned} \tag{27}$$

From (3), it can be derived that,

$$\begin{aligned} \frac{\partial C_{\text{p},i}}{\partial \lambda_{\text{i}}}\bigg|_{t=0} &= 3m_1\lambda_{0,i}^2 + 2m_2\lambda_{0,i} + m_3 \\ \frac{\partial^2 C_{\text{p},i}}{\partial \lambda_{\text{i}}^2}\bigg|_{t=0} &= 6m_1\lambda_{0,i} + 2m_2 \end{aligned} \tag{28}$$

where,

$$\lambda_{0,i} = \frac{\omega_{\text{r}0,i}R}{v_{\text{w},i}} \tag{29}$$

Objective 3 The third objective is to minimize the battery degradation caused by charging and discharging of the BESS. According to [35], the ESS degradation cost model can be expressed as,

$$BC = \frac{(P_{\text{ESS}}^{\text{ch}} + P_{\text{ESS}}^{\text{dis}})\mu_{\text{ESS}}\gamma_{\text{ESS}}T_{\text{c}}}{a_1[a_2(1-SOC^0)+a_3]e^{a_4 T_{\text{ESS}}}E_{\text{R}}(1-SOC^{\text{ref}})} \tag{30}$$

Therefore, the cost function of the third objective can be described by,

$$\text{Obj}_3 = \sum_{i=1}^{N_{\text{w}}}\sum_{k=1}^{N_{\text{p}}} \|BC(k)\|^2 \tag{31}$$

Accordingly, the overall cost function of the MPC-SIC is expressed as,

$$\begin{aligned} \min \quad &\lambda_\omega \sum_{i=1}^{N_{\text{w}}}\sum_{k=1}^{N_{\text{p}}} \left\|\Delta\omega_{\text{r},i}(k) - \Delta\omega_{\text{r,ave}}(k)\right\|^2 \\ &+\lambda_E \sum_{i=1}^{N_{\text{w}}}\sum_{k=1}^{N_{\text{p}}} E_{\text{loss},i}(k) + \lambda_B \sum_{k=1}^{N_{\text{p}}} \|BC(k)\|^2 \end{aligned} \tag{32}$$

The weighting coefficients of the three objectives λ_ω, λ_E and λ_B are determined through sensitivity analysis. To do this, the partial derivatives of the cost functions Obj_{1-3} with respect to the decision variable factor Δy of the MPC-SIC is firstly calculated and then the weighting coefficients are determined by setting priorities for these partial derivatives. In this paper, the priority ranking is $\text{Obj}_1 > \text{Obj}_2 > \text{Obj}_3$. Accordingly, the weighting coefficients are selected by,

$$\sum_{i=1}^{N_{\text{w}}}\left(\frac{\partial\Delta\omega_{\text{r},i}}{\partial y}\right)^2 \frac{\lambda_\omega}{N_{\text{w}}} > \sum_{i=1}^{N_{\text{w}}} \frac{\partial E_{\text{loss},i}}{\partial y}\frac{\lambda_E}{N_{\text{w}}} > \left(\frac{\partial BC}{\partial y}\right)^2 \lambda_B \tag{33}$$

4.3 Constraints

4.3.1 Constraints on active power output of WTs and BESS:

During the control process, the active power output of each WT is constrained by the WT generator's capacity, i.e.,

$$0 \le P_{\text{e}0,i} + \Delta P_{\text{ref},i} \le P_{\max,i},\ i = 1, 2, \ldots, N_{\text{w}} \tag{34}$$

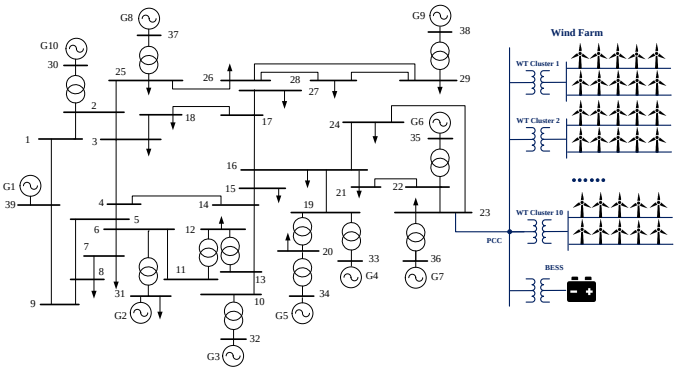

Fig. 4: Configuration of the test system.

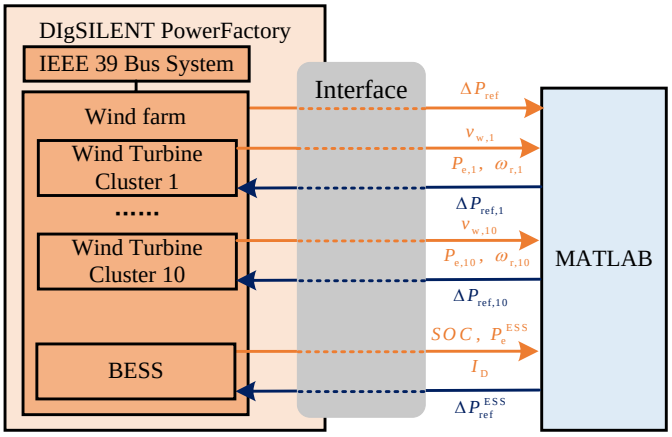

Fig. 5: Co-simulation framework between PowerFactory and MATLAB.

The BESS can operate in the charge or discharge mode, and its output power should follow the charge/discharge power limit, i.e.,

$$-P_{\text{discharge,max}}^{\text{ESS}} < P_{\text{e}}^{\text{ESS}} + \Delta P_{\text{ref}}^{\text{ESS}} < P_{\text{charge,max}}^{\text{ESS}} \tag{35}$$

4.3.2 Constraints on total incremental power of WF:

During MPC-SIC, the total incremental active power reference of the WF ΔP_{ref} is required to track the value calculated by the synthetic inertial controller, such that,

$$\sum_{i=1}^{N_{\text{w}}} \Delta P_{\text{ref},i} + \Delta P_{\text{ref}}^{\text{ESS}} = \Delta P_{\text{ref}} = K_{\text{p}}\Delta f + K_{\text{d}}\frac{\text{d}\Delta f}{\text{d}t} \tag{36}$$

The formulated MPC problem (32)-(36) can be transformed into a standard quadratic-programming (QP) problem and efficiently solved by commercial QP solvers in milliseconds.

5 Case Study

5.1 Test System

The proposed MPC-SIC is tested on a WF using DIgSILENT PowerFactory.

The WF consists of 100 WTs and a BESS. The WTs are divided into 10 clusters and the WTs in each cluster share the same wind speed profile which is generated using the four-component wind model proposed in [36]. The capacity of each WT is 5 MW, and the capacity of the BESS is 50 MW, thus the total capacity of the WF is 550 MW. The WF is connected to the IEEE 39 bus system at bus 23. Fig. 4 shows the configuration of the test system.

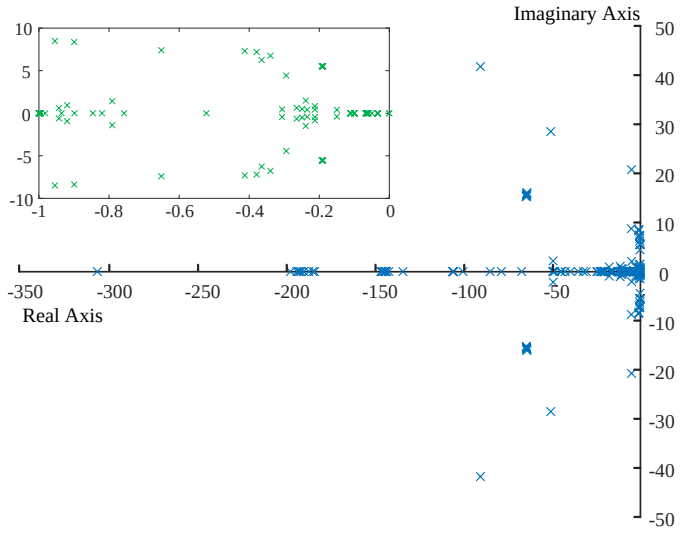

Fig. 6: Eigenvalues of the test system.

During the simulation, MPC-SIC is implemented as a MATLAB script and it is connected to a DSL model in the WF in PowerFactory through a co-simulation interface provided by PowerFactory. In this co-simulation framework, the MATLAB script is invoked at the beginning of every control period. It receives the operating conditions ($\omega_{\mathrm{r},i}$, $P_{\mathrm{e},i}$, $v_{\mathrm{w},i}$ measured at each WT, and SOC, $P_{\mathrm{e}}^{\mathrm{ESS}}$, i_{D} measured at the BESS), calculates the optimal active power references ($\Delta P_{\mathrm{ref},i}$ and $\Delta P_{\mathrm{ref}}^{\mathrm{ESS}}$), and then sends them to the WTs and BESS. The co-simulation framework between PowerFactory and MATLAB is shown in Fig. 5. The control period T_{c} is set as 0.5s.

At time $t = 20$s, the active power of load 4 is increased from 500 MW to 750 MW, causing a frequency excursion in the power system. MPC-SIC is activated at the same time to provide an inertial response. The total simulation time is 40 seconds. The results include the rotor speed of the WTs, loss of captured wind energy of the WF, degradation cost of the BESS, active power of the WTs/BESS /WF, and system frequency response. In order to test the performance of the proposed MPC-SIC, the conventional SIC is also implemented locally at the WTs and BESS, and the simulation results with MPC-SIC and conventional SIC are compared.

The stability of the test system with the MPC-SIC can be investigated by conducting eigenvalue analysis to the test system in DIgSILENT PowerFactory. The eigenvalues of the test system with the MPC-SIC are calculated and shown in Fig. 6. It can be seen from Fig. 6 that the eigenvalues of the test system are all located in the left half of the complex plane. Therefore, the test system is stable with the implementation of the MPC-SIC.

5.2 Simulation Results

5.2.1 Rotor speed: Figs. 7 and 8 show the rotor speeds of the WTs with the conventional SIC and MPC-SIC, respectively. Fig. 9 compares the minimum rotor speed of all WTs with the conventional SIC and MPC-SIC. Before the disturbance, the WTs operate in the MPPT mode and their rotor speeds vary because of the wind fluctuation. At $t = 20$s, the disturbance occurs, and the rotors of the WTs with conventional SIC begin to decelerate and extract the kinetic energy stored in the rotating masses to contribute to system frequency recovery. However, it can be seen from Fig. 8 that, after $t = 20$s, with the MPC-SIC, while some WTs' rotors begin to decelerate, some WTs' rotors under low wind speed conditions begin to accelerate. The acceleration is due to the first control objective of the MPC-SIC presented in 4.2, which is to minimize the difference among the rotor speeds of the WTs and it is achieved by assigning different $\Delta P_{\mathrm{ref},i}$ to the WTs. For the WTs operating in low wind speed conditions, to prevent their rotor speeds reaching the threshold, their $\Delta P_{\mathrm{ref},i}$ assigned by the MPC controller can be negative, which means that instead of extracting kinetic energy to the power

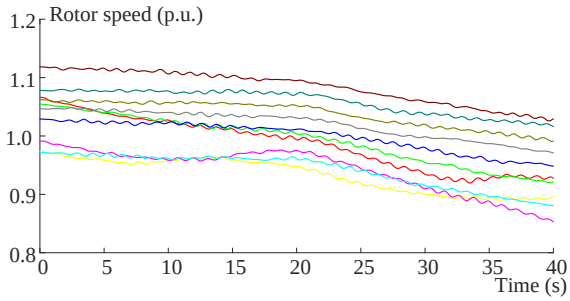

Fig. 7: Rotor speed of the WTs with conventional SIC.

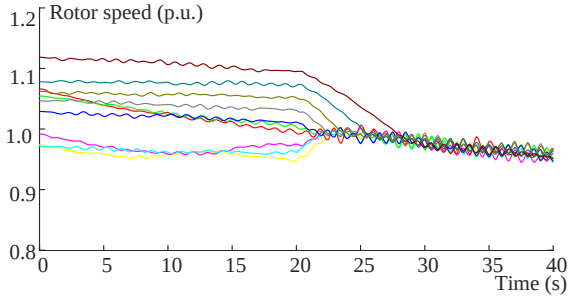

Fig. 8: Rotor speed of the WTs with MPC-SIC.

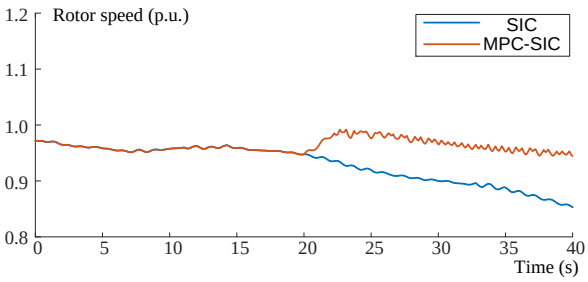

Fig. 9: Minimum rotor speed among all WTs with conventional SIC and with MPC-SIC.

system, these WTs should reserve more kinetic energy by decreasing their active power output. It can be seen from Fig. 9 that, during the control process, the minimum rotor speed among all WTs with the MPC-SIC is significantly improved, compared with conventional SIC. At $t = 40$s, the minimum rotor speed among all WTs with the conventional SIC reaches 0.85 p.u., while the minimum rotor speed among all WTs with the MPC-SIC is 0.94 p.u. With higher minimum rotor speed, the risk of abrupt termination of the SIC can be effectively reduced and the secondary frequency drop caused by the termination of the SIC can also be mitigated.

5.2.2 Loss of captured wind energy of WF and degradation cost of BESS: The losses of captured wind energy of the WF with the conventional SIC and MPC-SIC during each control period of MPC-SIC are compared in Fig. 10. The mean values of the loss of captured wind energy are 0.0559 kWh with the conventional SIC, and 0.0293 kWh with the MPC-SIC. The result shows

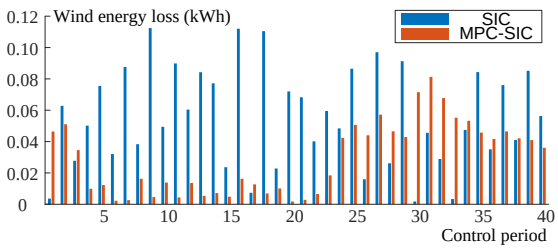

Fig. 10: Loss of captured wind energy of WF with conventional SIC and MPC-SIC.

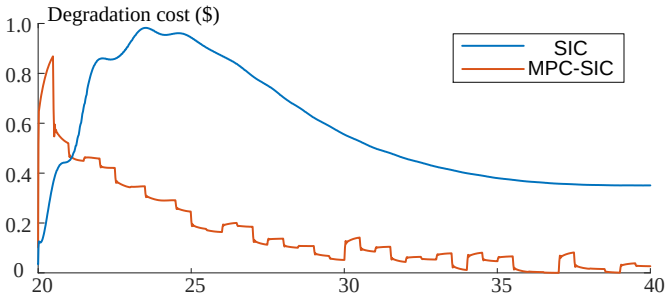

Fig. 11: Degradation cost of BESS with conventional SIC and MPC-SIC.

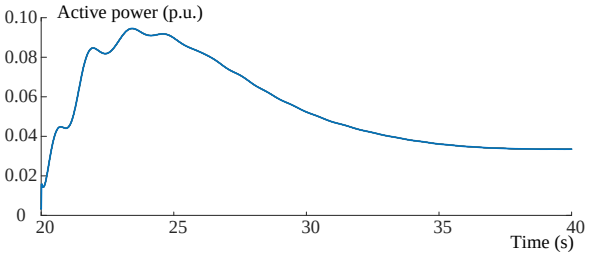

Fig. 12: Incremental active power references for WTs with conventional SIC.

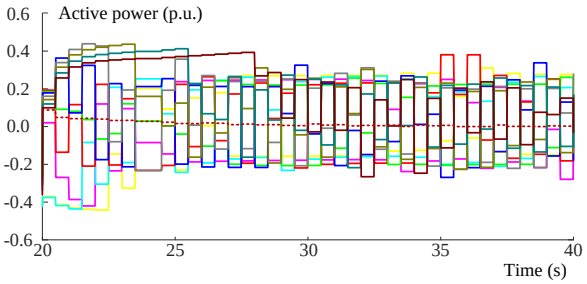

Fig. 13: Incremental active power references for WTs with MPC-SIC.

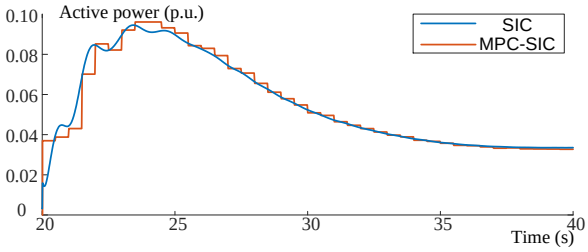

Fig. 14: Incremental active power references of the WF with conventional SIC and with MPC-SIC.

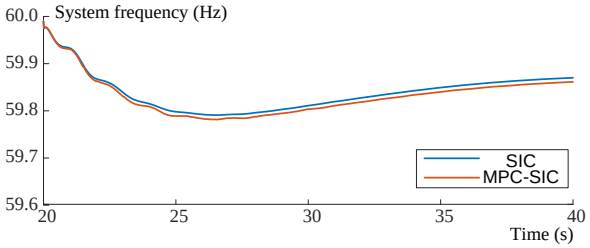

Fig. 15: System frequency responses with conventional SIC and with MPC-SIC.

that, compared with the conventional SIC, the wind energy loss can be significantly reduced with MPC-SIC, by 48% in this case. Therefore, the proposed MPC-SIC can improve the wind energy usage of the WF during the SIC.

The degradation cost of the BESS with the conventional SIC and MPC-SIC during each control period of MPC-SIC are compared in Fig. 11. The mean values of the degradation cost of BESS are 0.5776 $ with the conventional SIC, and 0.1625 $ with the MPC-SIC. Therefore, the degradation cost of BESS is significantly reduced with MPC-SIC, by 71.87% in this case. In this way, the lifetime of the BESS can be extended.

5.2.3 Active power: The incremental active power references of the WTs/BESS with the conventional SIC and MPC-SIC are shown in Fig. 12 and Fig. 13, respectively. The incremental active power references of the WF ΔP_{ref} with conventional SIC and with MPC-SIC are compared in Fig. 14. It can be seen from Fig. 12 that with conventional SIC, the incremental active power references of all WTs and the BESS are equal, because they are calculated locally at individual WTs and BESS with the same control parameters $(K_{\mathrm{p}}, K_{\mathrm{d}})$, regardless of operating conditions of the WTs and the BESS. However, with the MPC-SIC, the incremental power references of the WTs and the BESS are different from each other and also time-varying, since they are calculated and dispatched by the MPC controller in order to satisfy the control objectives for each control period.

On the other hand, from Fig. 14, it can be seen that there is not much difference between the ΔP_{ref} with conventional SIC and with MPC-SIC, because the equality constraint in 4.3 is used for the MPC controller to guarantee that the total active power output of the WF with MPC-SIC is equal to that with the conventional SIC.

5.2.4 System frequency response: The system frequency responses with conventional SIC and MPC-SIC are compared in Fig. 15. During the control process, the system frequency at the nadir with conventional SIC and with MPC-SIC are 59.79 Hz and 59.78 Hz, respectively, thus the difference is only 0.01 Hz. On the other hand, the initial RoCoF of the system with conventional SIC and with MPC-SIC are -0.32 Hz/s and -0.35 Hz/s, respectively. The difference is only 0.03 Hz/s. The difference of the system frequency

responses between SIC and MPC-SIC is caused by the difference of the total incremental active power of the WF as shown in Fig. 14. However, it is negligible. To achieve better control performance, the improvement of the system frequency response can be an objective of the MPC-SIC, which will be investigated in future work.

In summary, the simulation results prove that the MPC-SIC can effectively mitigate the secondary frequency drop and reduce the operation cost of the WF by improving the efficiency of wind energy usage and the lifetime of the BESS while maintaining the same total active power output of the WF and the system frequency response as those with the conventional SIC.

5.3 Robustness of MPC-SIC

The performance of the MPC-SIC can be affected by the wind penetration levels and disturbance magnitudes. Therefore, in order to show the effectiveness of the MPC-SIC over the conventional SIC in different conditions, 3 more cases were performed by varying these factors:

1. Case 1: wind penetration level is 20%, the active power of load 04 is increased by 400 MW at time $t = 20$s.
2. Case 2: Wind penetration level is 30%, the active power of load 39 is increased by 450 MW at time $t = 20$s.
3. Case 3: wind penetration level is 40%, the active power of load 39 is increased by 500 MW at time $t = 20$s.

The minimum rotor speed among all WTs, mean values of loss of captured wind energy and degradation cost of BESS with the MPC-SIC and conventional SIC are compared for the above three cases. The results are listed in Tables. 1-3.

As can be seen from Tables. 1-3, in Cases 1-3, compared with conventional SIC, the minimum rotor speed among all WTs with MPC-SIC can be improved by 0.09 p.u., 0.11 p.u. and 0.08 p.u., respectively. The loss of captured wind energy with MPC-SIC can be reduced by 12.25%, 46.54% and 64.42%, respectively. The degradation cost of BESS with MPC-SIC can be reduced by 83.43%, 83.05% and 77.43%, respectively. Thus, it can be concluded that the MPC-SIC is robust to different wind penetration levels and disturbances.

6 Conclusion

In this paper, an MPC based SIC is developed to optimize the performance of the SIC of a WF equipped with the BESS. The linearized predictive model of the WF consisting of WTs and a BESS is firstly derived in details. Afterwards, the MPC-SIC is designed for the WF based on the predictive model of the WF. Compared with the conventional SIC which is applied locally at the WTs/BESS, the proposed MPC-SIC is implemented at the WF level. Furthermore, the different operating conditions of the WTs and the BESS are measured and updated during each control period. Therefore, the MPC-SIC realizes the coordination of the WTs and the BESS and satisfies the control objectives by regulating their active power output.

As the simulation results show, compared with the conventional SIC, the minimum rotor speed among all WTs with MPC-SIC can be improved by 0.08-0.11 p.u. in different cases, which proves that the proposed MPC-SIC can effectively avoid the over-deceleration of the WTs so as to mitigate the secondary frequency drop of the power system. Furthermore, the loss of captured wind energy of WF with MPC-SIC can be reduced by 12%-64% and the degradation cost of the BESS with MPC-SIC can be reduced by 72%-83% in different cases. The results prove that, with the proposed MPC-SIC, the wind farm can reduce the operation cost of the WF by improving the efficiency of wind energy usage and lifetime of the BESS.

During the control process, the MPC problem formulated in this paper is solved at the MPC controller of the WF using centralized optimization algorithms. For large-scale WFs with large number of WTs, the MPC controller may suffer a heavy computational burden. Therefore, the MPC problem will be decomposed and then solved in a distributed manner to improve the computation efficiency in our future research.

Table 1 Comparison of Minimum rotor speed among all WTs (p.u.)

	Case 1	Case 2	Case 3
MPC-SIC	0.8408	0.7866	0.7118
SIC	0.9267	0.8703	0.7983

Table 2 Comparison of mean value of loss of captured wind energy (kWh)

	Case 1	Case 2	Case 3
MPC-SIC	0.0603	0.0737	0.0908
SIC	0.0687	0.1379	0.2551

Table 3 Comparison of mean value of degradation cost of BESS ($)

	Case 1	Case 2	Case 3
MPC-SIC	0.1118	0.1869	0.3645
SIC	0.6747	1.1027	1.6145

7 Acknowledgements

This work is supported by the National Key R&D Program of China (2018YFB0904000).

8 References

1 Nguyen, H.T., Yang, G., Nielsen, A.H., *et al.*: 'Combination of Synchronous Condenser and Synthetic Inertia for Frequency Stability Enhancement in Low Inertia Systems', *IEEE Trans. Sustain. Energy*, 2018, Available from: https://ieeexplore.ieee.org/document/8412562/

2 Morren, J., de Haan, S.W.H., Kling, W.L., *et al.*: 'Wind turbines emulating inertia and supporting primary frequency control', *IEEE Trans. Power Syst.*, 2006, **21**, (1), pp. 433–434

3 Wilches-Bernal, F., Chow, J.H., Sanchez.Gasca, J.J., *et al.*: 'A fundamental study of applying wind turbines for power system frequency control', *IEEE Trans. Power Syst.*, 2016, **31**, (2), pp. 1496–1505

4 Ullah, N.R., Thiringer, T., Karlsson, D.: 'Temporary primary frequency control support by variable speed wind turbines - Potential and applications', *IEEE Trans. Power Syst.*, 2008, **23**, (2), pp. 601–612

5 Kayikçi, M., Milanović, J.V.: 'Dynamic contribution of DFIG-based wind plants to system frequency disturbances', *IEEE Trans. Power Syst.*, 2009, **24**, (2), pp. 859–867

6 Clark, K., Miller, N.W., Sanchez.Gasca, J.J. 'Modeling of GE wind turbine-generators for grid studies', 2010. April

7 Stiesdal, H.: 'Wind energy installation and method of controlling the output power from a wind energy installation', *USPatent,* , US 8138621 B2, 2012.

8 Morren, J., Pierik, J., de Haan, S.W.H.: 'Inertial response of variable speed wind turbines', *Electr. Power Syst. Res.*, 2006, **76**, (11), pp. 980–987

9 Liu, F., Liu, Z., Mei, S., *et al.*: 'ESO-Based Inertia Emulation and Rotor Speed Recovery Control for DFIGs', *IEEE Trans. Energy Convers.*, 2017, **32**, (3), pp. 1209–1219

10 Azizipanah.Abarghooee, R., Malekpour, M., Dragicevic, T., *et al.*: 'A Linear Inertial Response Emulation for Variable Speed Wind Turbines', *IEEE Trans. Power Syst.*, 2019, in press

11 Bonfiglio, A., Invernizzi, M., Labella, A., *et al.*: 'Design and Implementation of a Variable Synthetic Inertia Controller for Wind Turbine Generators', *IEEE Trans. Power Syst.*, 2019, **34**, (1), pp. 754–764

12 Huang, L., Xin, H., Zhang, L., *et al.*: 'Synchronization and Frequency Regulation of DFIG-based Wind Turbine Generators with Synchronized Control', *IEEE Trans. Energy Convers.*, 2017, **32**, (3), pp. 1251–1262.

13 Hwang, M., Muljadi, E., Jang, G., *et al.*: 'Disturbance-Adaptive Short-Term Frequency Support of a DFIG Associated With the Variable Gain Based on the ROCOF and Rotor Speed', *IEEE Trans. Power Syst.*, 2017, **32**, (3), pp. 1873–1881.

14 Peng, X., Yao, W., Yan, C., *et al.*: 'Two-Stage Variable Proportion Coefficient Based Frequency Support of Grid-Connected DFIG-WTs', *IEEE Trans. Power Syst.*, 2019, in press.

15 Gloe, A., Jauch, C., Craciun, B., *et al.*: 'Continuous provision of synthetic inertia with wind turbines: implications for the wind turbine and for the grid', *IET Renew. Power Gen.*, 2019, **13**, (5), pp. 668–675

16 Markovic, U., Chu, Z., Aristidou, P., *et al.*: 'LQR-Based Adaptive Virtual Synchronous Machine for Power Systems With High Inverter Penetration', *IEEE Trans. Sustain. Energy*, 2019, **10**, (3), pp. 1501–1512.

17 Liu, Z., Shen, C., Liu, F., *et al.*: 'Speed recovery strategy for the inertia response control of DFIGs: extended state observer based approach', *IET Renew. Power Gen.*, 2017, **11**, (8), pp. 1110–1120.
18 Li, Y., Xu, Z., Wong, K.P.: 'Advanced Control Strategies of PMSG-Based Wind Turbines for System Inertia Support', *IEEE Trans. Power Syst.*, 2017, **32**, (4), pp. 3027–3037
19 Li, Y., Xu, Z., Zhang, J., *et al.*: 'Variable gain control scheme of DFIG-based wind farm for over-frequency support', *Renew. Energy*, 2018, **120**, pp. 379–391
20 Wang, Z., Wu, W.: 'Coordinated Control Method for DFIG-Based Wind Farm to Provide Primary Frequency Regulation Service', *IEEE Trans. Power Syst.*, 2018, **33**, (3), pp. 2644–2659
21 De Paola, A., Angeli, D., Strbac, G.: 'Scheduling of Wind Farms for Optimal Frequency Response and Energy Recovery', *IEEE Trans. Control Syst. Technol.*, 2016, **24**, (5), pp. 1764–1778
22 Jiang, Q., Gong, Y., Wang, H.: 'A battery energy storage system dual-layer control strategy for mitigating wind farm fluctuations', *IEEE Trans. Power Syst.*, 2013, **28**, (3), pp. 3263–3273
23 Zhao, H., Wu, Q., Guo, Q., *et al.*: 'Optimal active power control of a wind farm equipped with energy storage system based on distributed model predictive control', *IET Gener. Transm. Distrib.*, 2016, **10**, (3), pp. 669–677.
24 Fang, J., Zhang, R., Li, H., *et al.*: 'Frequency Derivative-based Inertia Enhancement by Grid-Connected Power Converters with a Frequency-Locked-Loop', *IEEE Trans. Smart Grid*, 2019, **10**, (5), pp. 4918–4927
25 Wu, Z., Gao, D.W., Zhang, H., *et al.*: 'Coordinated Control Strategy of Battery Energy Storage System and PMSG-WTG to Enhance System Frequency Regulation Capability', *IEEE Trans. Sustain. Energy*, 2017, **8**, (3), pp. 1330–1343.
26 Miao, L., Wen, J., Xie, H., *et al.*: 'Coordinated Control Strategy of Wind Turbine Generator and Energy Storage Equipment for Frequency Support', *IEEE Trans. Ind. Appl.*, 2015, **51**, (4), pp. 2732–2742
27 Peng, B., Zhang, F., Liang, J., *et al.*: 'Coordinated control strategy for the short-term frequency response of a DFIG-ES system based on wind speed zone classification and fuzzy logic control', *Int. J. Electr. Power Energy Syst.*, 2019, **107**, (December 2018), pp. 363–378.
28 El.Hameed, M.A., Elkholy, M.M., El.Fergany, A.A.: 'Efficient frequency regulation in highly penetrated power systems by renewable energy sources using stochastic fractal optimiser', *IET Renew. Power Gen.*, 2019, **13**, pp. 2174–2183
29 Stroe, D.I., Knap, V., Swierczynski, M., *et al.*: 'Operation of a grid-connected lithium-ion battery energy storage system for primary frequency regulation: A battery lifetime perspective', *IEEE Trans. Ind Appl.*, 2017, **53**, (1), pp. 430–438
30 Zhao, H., Wu, Q., Guo, Q., *et al.*: 'Distributed model predictive control of a wind farm for optimal active power controlpart I: Clustering-based wind turbine model linearization', *IEEE Trans. Sustain. Energy*, 2015, **6**, (3), pp. 831–839
31 Guo, Y., Gao, H., Wu, Q., *et al.*: 'Enhanced voltage control of VSC-HVDC-connected offshore wind farms based on model predictive control', *IEEE Trans. Sustain. Energy*, 2018, **9**, (1), pp. 474–487
32 Huang, S., Wu, Q., Guo, Y., *et al.*: 'Bi-level decentralised active power control for large-scale wind farm cluster', *IET Renew. Power Gen.*, 2018, **12**, (13), pp. 1486–1492
33 DIgSILENT GmbH: 'DIgSILENT PowerFactory Application Example Battery Energy Storing Systems', 2010
34 Wang, S., Tomsovic, K.: 'A Novel Active Power Control Framework for Wind Turbine Generators to Improve Frequency Response', *IEEE Trans. Power Syst.*, 2018, **33**, (6), pp. 6579–6589.
35 Huang, S., Wu, Q., Guo, Y., *et al.*: 'Hierarchical active power control of DFIG-based wind farm with distributed energy storage systems based on ADMM', *IEEE Trans. Sustain. Energy*, in press.
36 Anderson, P., Bose, A.: 'Stability Simulation Of Wind Turbine Systems', *IEEE Trans. Power App. Syst.*, 1983, **PAS-102**, (12), pp. 3791–3795